

Search for the light hadron decay $\chi_{c1}(3872) \rightarrow \pi^+ \pi^- \eta$ M. Ablikim *et al.**
(BESIII Collaboration) (Received 26 August 2023; accepted 6 December 2023; published 29 January 2024)

With a data sample corresponding to an integrated luminosity of 11.5 fb^{-1} collected with the BESIII detector operating at the BEPCII storage ring, for the first time the light hadron decay $\chi_{c1}(3872) \rightarrow \pi^+ \pi^- \eta$ is searched for. While no significant signal is observed, the upper limits at the 90% confidence level for $\sigma[e^+e^- \rightarrow \gamma\chi_{c1}(3872)]\mathcal{B}[\chi_{c1}(3872) \rightarrow \pi^+ \pi^- \eta]$ at center of mass energies from 4.13 GeV to 4.34 GeV are determined. By normalizing to the $\chi_{c1}(3872) \rightarrow \pi^+ \pi^- J/\psi$ decay channel, a 90% confidence level upper limit for the branching fraction ratio $\mathcal{R} = \mathcal{B}[\chi_{c1}(3872) \rightarrow \pi^+ \pi^- \eta]/\mathcal{B}[\chi_{c1}(3872) \rightarrow \pi^+ \pi^- J/\psi] < 0.12$ is given. These measurements provide important inputs for understanding the internal structure of the $\chi_{c1}(3872)$ resonance.

DOI: [10.1103/PhysRevD.109.L011102](https://doi.org/10.1103/PhysRevD.109.L011102)

Since its discovery in 2003 [1], the $\chi_{c1}(3872)$ resonance has been widely considered an exotic hadron state beyond the conventional baryon and meson picture [2]. At the moment, several theoretical models have been proposed that describe the $\chi_{c1}(3872)$ as a tetraquark state [3], a P -wave radially excited charmonium state [4], or a $D^0 \bar{D}^{*0}$ meson molecule [5,6], the latter one being favored due to the $\chi_{c1}(3872)$ mass being very close to the $D^0 \bar{D}^{*0}$ mass threshold [7]. However, the production rate of $\chi_{c1}(3872)$ in high energy $pp/p\bar{p}$ collisions is comparable to that of the $\psi(2S)$ [8], which does not agree with a pure molecule prediction [9]. To explain this, the $\chi_{c1}(3872)$ has been proposed to be a charmonium-hadronic molecule mixture state [10].

Many experimental measurements have investigated the mass, width [7], spin-parity [11,12] and decays [13–18] of the $\chi_{c1}(3872)$. The branching fractions (BFs) of several final states involving charmonium or the $D^{(*)}$ meson, such as $\pi^+ \pi^- J/\psi$, $\omega J/\psi$, $\gamma J/\psi$, $\pi^0 \chi_{c1}$, and $D^0 \bar{D}^{*0}$ have been measured [7]. Yet, no decay final state without charm, such as light hadrons has been observed, except for an evidence of $\gamma\gamma^*$ production [19]. Theoretically, if the $\chi_{c1}(3872)$ was a $D^0 \bar{D}^{*0}$ molecular state, its size would be very large ($\sim 10 \text{ fm}$) due to a small binding energy [6] and the c and \bar{c} quarks would be expected to be far away from each other. Consequently, the light hadron decay of $\chi_{c1}(3872)$, which requires $c\bar{c}$ annihilation [5,20], would be suppressed.

If, however, the $\chi_{c1}(3872)$ wave function contains a sizeable $c\bar{c}$ core component, the BFs of these final states will be enhanced.

To further understand the nature of the $\chi_{c1}(3872)$, more experimental studies about its decay channels are required. By taking measurements from several experiments into account, Ref. [21] has performed a global analysis on the BFs of its decays, which indicates that $(32_{-32}^{+18})\%$ of the BFs have not yet been observed in experiment. The BESIII experiment accumulated the world's largest e^+e^- annihilation data from $\sqrt{s} = 4.01 \text{ GeV}$ to 4.95 GeV and offers an opportunity to further investigate decays of $\chi_{c1}(3872)$, shedding light on the wave function of the $\chi_{c1}(3872)$ state. Previously, the BESIII Collaboration has already established the $e^+e^- \rightarrow \gamma\chi_{c1}(3872)$ production method with large significance [14,15].

In this paper, based on the assumption that $\chi_{c1}(3872)$ contains a sizeable component of the $\chi_{c1}(2P)$, we search for the light hadron decay process $\chi_{c1}(3872) \rightarrow \pi^+ \pi^- \eta$, where the $\chi_{c1}(3872)$ particle is produced via the radiative transition $e^+e^- \rightarrow \gamma\chi_{c1}(3872)$. The η candidate is reconstructed via its $\gamma\gamma$ and $\pi^+ \pi^- \pi^0 (\rightarrow \gamma\gamma)$ decays. A data sample taken at center of mass (c.m.) energy from $\sqrt{s} = 4.13 \text{ GeV}$ to 4.34 GeV [22,23] is used, corresponding to an integrated luminosity of 11.5 fb^{-1} [24,25], see Table I.

The BESIII detector [26] records symmetric e^+e^- collisions provided by the BEPCII storage ring [27], which operates in the c.m. energy range from 2.0 GeV to 4.95 GeV. BESIII has collected large data samples in this energy region [28]. The cylindrical core of the BESIII detector covers 93% of the full solid angle and consists of a helium-based multilayer drift chamber (MDC), a plastic scintillator time of flight (TOF) system, and a CsI(Tl) electromagnetic calorimeter (EMC), which are all enclosed in a superconducting solenoidal magnet providing a 1.0 T (0.9 T in

*Full author list given at the end of the Letter.

2012) magnetic field. The solenoid is supported by an octagonal flux-return yoke with resistive-plate counter muon identification modules interleaved with steel. The charged-particle momentum resolution at 1 GeV/ c is 0.5%, and the dE/dx resolution is 6% for electrons from Bhabha scattering. The EMC measures photon energies with a resolution of 2.5% (5%) at 1 GeV in the barrel (end cap) region. The time resolution in the TOF barrel region is 68 ps, while that in the end cap region is 110 ps. The end cap TOF system was upgraded in 2015 using multigap resistive plate chamber technology, providing a time resolution of 60 ps [29].

Simulated data samples produced with a Geant4-based [30] Monte Carlo (MC) package, which includes the geometric description of the BESIII detector and the detector response, are used to determine detection efficiencies, optimize event selection, and estimate backgrounds. For the signal process, 100,000 $e^+e^- \rightarrow \gamma\chi_{c1}(3872)$ events are generated at each c.m. energy, assuming an $E1$ radiative transition process which has been verified by BESIII data [17]. The possible initial-state radiation (ISR) is simulated with KKMC [31], incorporating the \sqrt{s} -dependent production cross section of $e^+e^- \rightarrow \gamma\chi_{c1}(3872)$ [17]. The maximum ISR photon energy is set according to the production threshold (3.9 GeV) of the $\gamma\chi_{c1}(3872)$ system. The decay of $\chi_{c1}(3872) \rightarrow \pi^+\pi^-\eta$ and $\eta \rightarrow \gamma\gamma$ is generated by EvtGen [32] with the phase-space model. The other decay $\eta \rightarrow \pi^+\pi^-\pi^0$ is generated according to the Dalitz distribution measured by BESIII [33]. The final-state radiation of charged particles is simulated with the PHOTOS package [34].

To study the possible background, an inclusive MC sample is used, including the production of open charm processes, the ISR production of vector charmonium(like) states, and the continuum processes incorporated in KKMC [31]. All particle decays are modeled with EvtGen [32] using BFs taken from the Particle Data Group (PDG) [7], when available, or otherwise modeled with LUNDCHARM [35] for charmonium states and PYTHIA [36] for other hadrons. The equivalent luminosity of the inclusive MC sample is 10 times that of data at $\sqrt{s} = 4178.0$ MeV, and is of equal size to data at other c.m. energies.

Charged tracks detected in the MDC are required to be within a polar angle (θ) range of $|\cos\theta| < 0.93$, where θ is defined with respect to the z -axis, which is the symmetry axis of the MDC. For each charged track, the distance of closest approach to the interaction point must be less than 10 cm along the z -axis, $|V_z|$, and less than 1 cm in the transverse plane, $|V_{xy}|$. Photon candidates are identified using showers in the EMC. The deposited energy of each shower must be more than 25 MeV in the barrel region ($|\cos\theta| < 0.80$) and more than 50 MeV in the end cap region ($0.86 < |\cos\theta| < 0.92$). To exclude showers that originate from charged tracks, the angle subtended by the EMC shower and the position of the closest charged track at the EMC must be greater than 10 degrees. To suppress electronic noise and showers unrelated to the event, the

EMC time with respect to the event start time is required to be within [0, 700] ns.

For the process of $e^+e^- \rightarrow \gamma\chi_{c1}(3872) \rightarrow \gamma\pi^+\pi^-\eta$ with $\eta \rightarrow \gamma\gamma$, the number of charged tracks is required to be two with zero net charge in an event, and both tracks are assigned as pion candidates. We also require at least three good photon candidates for each event. To improve the resolution and reduce backgrounds, a five-constraint (5C) kinematic fit is performed. Four constraints come from the four-momentum conservation of the final state particles equal to the initial e^+e^- colliding beams, and the additional one comes from the η mass. For possible multicomination of photon candidates, the one with the minimum χ_{5C}^2 is retained, and $\chi_{5C}^2 < 16$ is further required. This value is determined by optimizing the figure of merit (FOM) $S/\sqrt{S+B}$, where S represents the number of signal events from signal MC simulation, and B is the number of background events estimated from the inclusive MC sample.

By analyzing the inclusive MC sample, we find that there are miscombination backgrounds from $\pi^0 \rightarrow \gamma\gamma$ decays. To reduce these background events, $|M(\gamma_{\text{rad}}\gamma_{1(2)}) - m(\pi^0)| > 20$ MeV/ c^2 is required, where γ_{rad} refers to the radiative photon in $e^+e^- \rightarrow \gamma\chi_{c1}(3872)$, $\gamma_{1(2)}$ denote the two photons from η decay, $M(\gamma_{\text{rad}}\gamma_{1(2)})$ is the invariant mass of γ_{rad} and $\gamma_{1(2)}$ combination, and $m(\pi^0)$ is the nominal mass of π^0 [7]. In addition, there are also possible background events from the radiative dimuon [$e^+e^- \rightarrow (\gamma)\mu^+\mu^-$] process, which is removed by requiring the opening angle between pion pair to fulfill $\cos\theta_{\pi^+\pi^-} > -0.96$. After imposing these event selection criteria, the distribution of $M(\pi^+\pi^-\eta)$ from the full dataset is shown in Fig. 1(a). No $\chi_{c1}(3872)$ signal is observed, and the background contribution estimated from the inclusive MC sample shows no peaking structure in the signal region.

For the process of $e^+e^- \rightarrow \gamma\chi_{c1}(3872) \rightarrow \gamma\pi^+\pi^-\eta$ with $\eta \rightarrow \pi^+\pi^-\pi^0$ and $\pi^0 \rightarrow \gamma\gamma$, the number of charged tracks is required to be four with zero net charge in an event. Due to possible kaon background contamination, particle identification (PID) for charged tracks, combining measurements of the ionization energy loss (dE/dx) in the MDC and the flight time in the TOF to evaluate the likelihoods $\mathcal{L}(h)$ ($h = p, K, \pi$) for each hadron (h) hypothesis, is applied. At least one of the pion candidates is required to satisfy $\mathcal{L}(\pi) > \mathcal{L}(K)$. We also require at least three good photon candidates for each event. To improve the resolution and reduce backgrounds, a 5C kinematic fit is performed, where four constraints come from the four-momentum conservation of the final state particles equal to the initial e^+e^- colliding beams, and the additional one comes from the η mass. For possible multicomination due to multipion and multiphoton candidates in an event, the one with the minimum χ_{5C}^2 is retained and $\chi_{5C}^2 < 30$ is further required. This value is determined by optimizing the FOM.

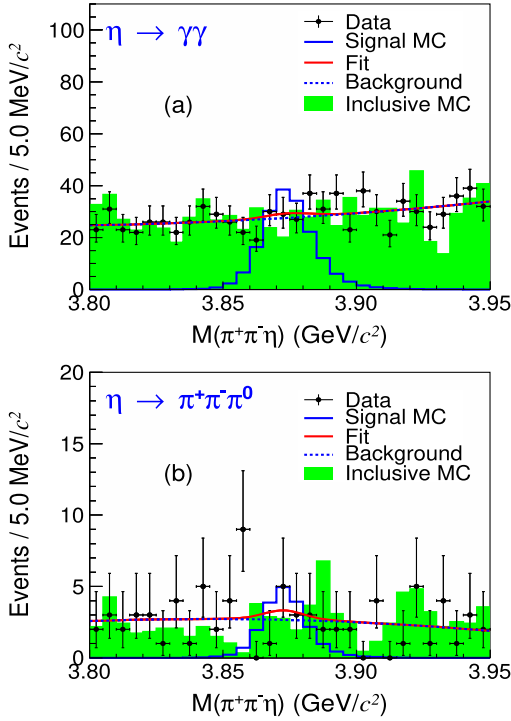


FIG. 1. The $M(\pi^+\pi^-\eta)$ distributions from $\eta \rightarrow \gamma\gamma$ mode (a) and $\pi^+\pi^-\pi^0$ mode (b) with fit curves overlaid. Dots with error bars are data, the blue solid curves are the MC signal with arbitrary normalization, the red solid curves are the fit result, the blue dashed curves are the background components, and the green shaded histograms are the backgrounds estimated from the inclusive MC sample.

The π^0 mass window is defined as $|M(\gamma\gamma) - m(\pi^0)| < 19.6 \text{ MeV}/c^2$ ($\pm 3\sigma$ around the π^0 mass).

Through the study of the inclusive MC sample, we find that the main backgrounds come from $e^+e^- \rightarrow \pi^+\pi^-\pi^0$. Events satisfying $125.6 \text{ MeV}/c^2 < M(\gamma_{\text{rad}}\gamma_1) < 150.0 \text{ MeV}/c^2$ and $115.7 \text{ MeV}/c^2 < M(\gamma_{\text{rad}}\gamma_2) < 160.0 \text{ MeV}/c^2$ are rejected to suppress this background, where $\gamma_{1(2)}$ denote the two photons from π^0 decay (sorted by energies) and $M(\gamma_{\text{rad}}\gamma_{1(2)})$ is the invariant mass of γ_{rad} and $\gamma_{1(2)}$ combination. The different mass window vetos are optimized by FOM. After imposing the selection criteria above, the obtained $M(\pi^+\pi^-\eta)$ distribution from the full dataset is shown in Fig. 1(b). There is no obvious $\chi_{c1}(3872)$ signal observed, and the background level is lower than that of the $\eta \rightarrow \gamma\gamma$ mode. The background also produces a smooth distribution in the signal region from the study of the inclusive MC sample.

For the two decay channels of η , a simultaneous fit to the $M(\pi^+\pi^-\eta)$ distribution is performed to extract the signal yield at each c.m. energy. In the fit, the signal probability density function is parametrized with an MC simulated shape [with $\chi_{c1}(3872)$ mass and width taken from PDG [7]], convolved with a Gaussian function which represents the resolution difference between data and MC

simulation. The mean and standard deviation of the Gaussian function are fixed to the values obtained from a control sample of $\chi_{c1}(1P) \rightarrow \pi^+\pi^-\eta$. The background shape is parametrized as a second-order polynomial function. In the simultaneous fit, the production rate for $e^+e^- \rightarrow \gamma\chi_{c1}(3872) \rightarrow \gamma\pi^+\pi^-\eta$ is a common parameter, and the signal yields for $\eta \rightarrow \gamma\gamma$ and $\pi^+\pi^-\pi^0$ modes are weighted according to the detection efficiencies and BFs. The fit results to the full dataset are shown in Fig. 1, and Figs. 4 and 5 in Appendix A show the fit results at each c.m. energy.

The production cross section $\sigma[e^+e^- \rightarrow \gamma\chi_{c1}(3872)]$ times the BF $\mathcal{B}[\chi_{c1}(3872) \rightarrow \pi^+\pi^-\eta]$ is calculated as

$$\sigma[e^+e^- \rightarrow \gamma\chi_{c1}(3872)]\mathcal{B}[\chi_{c1}(3872) \rightarrow \pi^+\pi^-\eta] = \frac{N_i^{\text{obs}}}{\mathcal{L}_{\text{int}}(1+\delta)(\varepsilon_1\mathcal{B}_1 + \varepsilon_2\mathcal{B}_2)} = \frac{N_i^{\text{sig}}}{\mathcal{L}_{\text{int}}(1+\delta)}, \quad (1)$$

where N_i^{obs} is the number of observed signal events from the i th dataset, \mathcal{L}_{int} is the corresponding integrated luminosity, $(1+\delta)$ is the radiative correction factor calculated by the KKMC MC generator [31], $\varepsilon_j\mathcal{B}_j$ ($j = 1, 2$) is the product of detection efficiency and BF for the $\eta \rightarrow \gamma\gamma$ and $\pi^+\pi^-\pi^0$ modes, and N_i^{sig} is the number of produced signal events after considering the detection efficiencies and BFs. Since no obvious signal is seen in the $M(\pi^+\pi^-\eta)$ distribution, an upper limit for $\sigma[e^+e^- \rightarrow \gamma\chi_{c1}(3872)]\mathcal{B}[\chi_{c1}(3872) \rightarrow \pi^+\pi^-\eta]$ is set using the Bayesian approach [37]. By scanning the likelihood function $\mathcal{L}(n)$ in the fit, the number of events corresponding to 90% of the integral $\int_0^{N^{\text{up}}} \mathcal{L}(n)dn = 0.9$ ($\int_0^{+\infty} \mathcal{L}(n)dn = 1$) is estimated as the upper limit (N^{up}) for the signal yield. The systematic uncertainty is considered by applying a Gaussian (with standard deviation equal to the total systematic uncertainty) smearing to the likelihood function. The upper limits $(\sigma[e^+e^- \rightarrow \gamma\chi_{c1}(3872)]\mathcal{B}[\chi_{c1}(3872) \rightarrow \pi^+\pi^-\eta])^{\text{up}}$ at 90% C.L. are measured from $\sqrt{s} = 4128.8 \text{ MeV}$ to 4337.9 MeV and are shown in Fig. 2 (corresponding numerical results are listed in Table I).

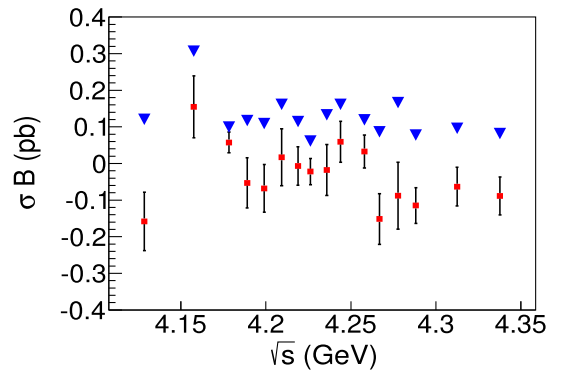


FIG. 2. The production cross section of $e^+e^- \rightarrow \gamma\chi_{c1}(3872)$ times the BF of $\chi_{c1}(3872) \rightarrow \pi^+\pi^-\eta$ as a function of c.m. energy. Blue triangles are the upper limit for $(\sigma\mathcal{B})^{\text{up}}$ at 90% C.L., and the red dots with error bars are the nominal result.

TABLE I. The production cross section of $e^+e^- \rightarrow \gamma\chi_{c1}(3872)$ times $\mathcal{B}[\chi_{c1}(3872) \rightarrow \pi^+\pi^-\eta]$. Here \sqrt{s} is the c.m. energy of dataset, \mathcal{L}_{int} is the integrated luminosity, $\varepsilon_{\eta \rightarrow \gamma\gamma(\pi^+\pi^-\pi^0)}$ is detection efficiency for $\eta \rightarrow \gamma\gamma(\pi^+\pi^-\pi^0)$ modes, $(1 + \delta)$ is the radiative correction factor, N_{sig} is the efficiency and branching fraction corrected production yield of $\chi_{c1}(3872) \rightarrow \pi^+\pi^-\eta$ signal events in $e^+e^- \rightarrow \gamma\chi_{c1}(3872)$ and $N_{\text{sig}}^{\text{up}}$ is the corresponding upper limit at the 90% C.L., $(\sigma\mathcal{B})$ is the product of the cross section $\sigma[e^+e^- \rightarrow \gamma\chi_{c1}(3872)]$ and BF $\mathcal{B}[\chi_{c1}(3872) \rightarrow \pi^+\pi^-\eta]$ and $(\sigma\mathcal{B})^{\text{up}}$ is the corresponding upper limit at the 90% C.L., and Δ denotes the total systematic uncertainty in the cross section measurement.

| \sqrt{s} (MeV) | \mathcal{L}_{int} (pb $^{-1}$) | $\varepsilon_{\eta \rightarrow \gamma\gamma}$ (%) | $\varepsilon_{\eta \rightarrow \pi^+\pi^-\pi^0}$ (%) | $(1 + \delta)$ | N_{sig} | $(\sigma\mathcal{B})$ (pb) | $N_{\text{sig}}^{\text{up}}$ | $(\sigma\mathcal{B})^{\text{up}}$ (pb) | Δ (%) |
|------------------|--|---|--|----------------|------------------|----------------------------|------------------------------|--|--------------|
| 4128.8 \pm 0.4 | 401.5 | 23.1 | 13.3 | 0.78 | -49.7 \pm 25.1 | -0.16 \pm 0.08 | 38.0 | 0.12 | 7.2 |
| 4157.8 \pm 0.3 | 408.7 | 23.7 | 13.5 | 0.78 | 49.1 \pm 26.9 | 0.15 \pm 0.08 | 97.2 | 0.31 | 7.2 |
| 4178.0 \pm 0.8 | 3194.5 | 22.7 | 13.2 | 0.78 | 143.1 \pm 70.3 | 0.06 \pm 0.03 | 247.0 | 0.10 | 7.6 |
| 4189.1 \pm 0.3 | 570.0 | 23.0 | 13.5 | 0.79 | -23.7 \pm 30.7 | -0.05 \pm 0.07 | 52.5 | 0.12 | 7.0 |
| 4199.2 \pm 0.3 | 526.7 | 23.3 | 13.8 | 0.80 | -28.6 \pm 27.3 | -0.07 \pm 0.06 | 46.0 | 0.11 | 7.8 |
| 4209.4 \pm 0.3 | 572.1 | 22.8 | 13.4 | 0.82 | 7.9 \pm 36.4 | 0.02 \pm 0.08 | 75.6 | 0.16 | 6.9 |
| 4218.9 \pm 0.3 | 569.2 | 22.7 | 13.5 | 0.84 | -3.1 \pm 25.1 | -0.01 \pm 0.05 | 54.9 | 0.12 | 7.9 |
| 4226.3 \pm 0.7 | 1100.9 | 22.6 | 13.4 | 0.86 | -20.9 \pm 34.0 | -0.02 \pm 0.04 | 58.2 | 0.06 | 7.5 |
| 4235.8 \pm 0.3 | 530.3 | 21.7 | 13.2 | 0.89 | -8.4 \pm 32.7 | -0.02 \pm 0.07 | 62.7 | 0.13 | 7.8 |
| 4244.0 \pm 0.3 | 594.0 | 21.4 | 12.8 | 0.92 | 32.5 \pm 30.6 | 0.06 \pm 0.06 | 88.2 | 0.16 | 7.6 |
| 4258.0 \pm 0.7 | 828.4 | 20.3 | 12.4 | 0.97 | 26.4 \pm 36.0 | 0.03 \pm 0.04 | 96.0 | 0.12 | 6.9 |
| 4266.8 \pm 0.3 | 529.7 | 19.9 | 11.9 | 1.00 | -80.6 \pm 36.8 | -0.15 \pm 0.07 | 46.0 | 0.09 | 6.7 |
| 4277.8 \pm 0.5 | 175.7 | 18.8 | 11.4 | 1.05 | -16.1 \pm 16.8 | -0.09 \pm 0.09 | 30.6 | 0.17 | 6.2 |
| 4288.4 \pm 0.3 | 498.5 | 18.8 | 11.0 | 1.09 | -62.2 \pm 26.3 | -0.11 \pm 0.05 | 42.0 | 0.08 | 7.7 |
| 4312.7 \pm 0.4 | 499.2 | 17.2 | 10.2 | 1.18 | -37.2 \pm 31.1 | -0.06 \pm 0.05 | 56.7 | 0.10 | 7.4 |
| 4337.9 \pm 0.4 | 511.5 | 16.1 | 9.3 | 1.28 | -58.1 \pm 33.9 | -0.09 \pm 0.05 | 53.7 | 0.08 | 7.2 |

The systematic uncertainties in the cross section measurement come from integrated luminosity measurements, photon detection, tracking efficiencies, PID, η/π^0 reconstruction, kinematic fit, quoted BFs, radiative correction factor, signal extraction, and MC decay model.

The integrated luminosities of the datasets are measured using large-angle Bhabha scattering events, with a systematic uncertainty of 0.66% [38]. The photon detection uncertainty is estimated to be 1.0% per photon by studying $J/\psi \rightarrow \rho\pi$ events [39]. The tracking efficiency uncertainty is estimated to be 1.0% per pion by studying $J/\psi \rightarrow p\bar{p}\pi^+\pi^-$ events [40]. For the decay with $\eta \rightarrow \pi^+\pi^-\pi^0$, we use PID for the pion selection, and at least one of the pion candidates is required to be identified. The PID efficiency of pions can be calculated as $1 - (1 - p)^4$, where p represents the PID efficiency for a single pion. Since p is very high (> 0.8) at BESIII, the uncertainty due to PID can be safely ignored [41].

The systematic uncertainty due to η/π^0 reconstruction is estimated to be 1.0% per η/π^0 , by studying a high-purity control sample of $J/\psi \rightarrow \bar{p}p\eta$ ($\bar{p}p\pi^0$) events [42]. For the uncertainty from the kinematic fit, we use a helix parameter correction method [43]. A correction is performed on the track parameters and half of the efficiency difference with and without the correction is taken as the systematic uncertainty.

For the radiative correction factor calculation, the cross section of $e^+e^- \rightarrow \gamma\chi_{c1}(3872)$ is input from Ref. [17], where a Breit-Wigner resonance $Y(4200)$ ($M[Y(4200)] =$

$4200.6_{-13.3}^{+7.9} \pm 3.0$ MeV/ c^2 and $\Gamma[Y(4200)] = 115_{-26}^{+38} \pm 12$ MeV) is employed to describe the cross section line shape. To estimate the potential effect due to the uncertainty of the resonance, a two-dimensional Gaussian sampling (possible correlation has been considered) method is used. We generate 300 groups of $Y(4200)$ resonance parameters (mass and width) and recalculate the $(1 + \delta)\varepsilon$. With the weighting method given in Ref. [44], we get the distribution of $(1 + \delta)\varepsilon$ according to the Gaussian sampling. A fit to this distribution yields the standard deviation of $(1 + \delta)\varepsilon$, which is taken as the corresponding systematic uncertainty.

In the nominal analysis, we use pure phase space to model the $\chi_{c1}(3872) \rightarrow \pi^+\pi^-\eta$ decay. As $\chi_{c1}(3872)$ is a $J^{PC} = 1^{++}$ resonance, we also try to model its decay by referring to a 1^{++} charmonium state $\chi_{c1}(1P)$. By selecting a pure control sample $\psi(2S) \rightarrow \gamma\chi_{c1}(1P)$ with $\chi_{c1}(1P) \rightarrow \pi^+\pi^-\eta$ from the BESIII data [45], we take the decay model of $\chi_{c1}(1P) \rightarrow \pi^+\pi^-\eta$ as an alternative, and the efficiency difference compared to the phase space model is taken as the associated systematic uncertainty.

The BFs of η/π^0 decays are taken from PDG [7], and the uncertainties are 0.5% for $\mathcal{B}(\eta \rightarrow \gamma\gamma)$, 1.22% for $\mathcal{B}(\eta \rightarrow \pi^+\pi^-\pi^0)$, and 0.03% for $\mathcal{B}(\pi^0 \rightarrow \gamma\gamma)$, respectively.

The systematic uncertainty due to signal extraction is dominated by the signal and background shapes. For the signal shape, the $\chi_{c1}(3872)$ is simulated with resonance parameters (mass and width) taken from PDG. We vary the resonance parameters by $\pm 1\sigma$ in the simulation. The background shape is varied from a first-order polynomial to a second-order polynomial. By repeating these fits, we

conservatively take the largest upper limit for signal yield as the final result.

Table III in Appendix B summarizes the systematic uncertainties at each c.m. energy. To combine the systematic uncertainties between two η decay modes, a weighted average is taken as

$$\Delta_{\text{tot}}^2 = \sum_{i=1}^2 \omega_i^2 \Delta_i^2 + 2 \sum_{i \neq j} \text{cov}(i, j), \quad (2)$$

$$\omega_i = \frac{\epsilon_i \mathcal{B}_i}{\sum_{i=1}^2 \epsilon_i \mathcal{B}_i}, \quad \text{cov}(i, j) = \rho_{ij} \omega_i \omega_j \Delta_i \Delta_j, \quad (3)$$

where Δ_{tot} is the combined total systematic uncertainty for each source, ω_i and Δ_i are the corresponding weight and systematic uncertainty, ϵ_i and \mathcal{B}_i are the efficiency and BF for the i th decay mode of η , and ρ_{ij} is the correlation coefficient between them. We take $\rho_{ij} = 1$ for the same systematic source, otherwise $\rho_{ij} = 0$.

Assuming all these sources are independent, the total systematic uncertainties are added in quadrature for different sources. Table I lists the total systematic uncertainties in the cross section measurement.

As the $e^+e^- \rightarrow \gamma\chi_{c1}(3872) \rightarrow \gamma\pi^+\pi^-J/\psi$ process has been observed at BESIII [14,15,17], we also measure the BF ratio $\mathcal{R} = \frac{\mathcal{B}[\chi_{c1}(3872) \rightarrow \pi^+\pi^-\eta]}{\mathcal{B}[\chi_{c1}(3872) \rightarrow \pi^+\pi^-J/\psi]}$, which is calculated as

$$\mathcal{R} = \frac{N_{\text{total}} \sum_i \mathcal{L}_i \sigma_i (1 + \delta_i) \epsilon'_i \mathcal{B}(J/\psi \rightarrow \ell^+ \ell^-)}{N'_{\text{total}} \sum_i \mathcal{L}_i \sigma_i (1 + \delta_i) (\epsilon_i^{\gamma\gamma} \mathcal{B}_1 + \epsilon_i^{\pi^+\pi^-\pi^0} \mathcal{B}_2)}, \quad (4)$$

where N_{total} is the total number of observed $\chi_{c1}(3872)$ signal events, σ_i is the $e^+e^- \rightarrow \gamma\chi_{c1}(3872)$ production cross section [17], \mathcal{L}_i , $(1 + \delta_i)$, and ϵ_i are the integrated luminosity, radiative correction factor, and efficiency at the i th c.m. energy, respectively (cf. Table I), and $\mathcal{B}_{1,2}$ are BFs of $\eta \rightarrow \gamma\gamma$ and $\eta \rightarrow \pi^+\pi^-\pi^0$. The unprimed variables are for $\chi_{c1}(3872) \rightarrow \pi^+\pi^-\eta$ and the primed variables are for $\chi_{c1}(3872) \rightarrow \pi^+\pi^-J/\psi$. Note that the integrated luminosity, the $e^+e^- \rightarrow \gamma\chi_{c1}(3872)$ production cross section σ_i , and the radiative correction factor are the same for both processes.

Since we do not observe any obvious signal in the $\chi_{c1}(3872) \rightarrow \pi^+\pi^-\eta$ decay, an upper limit at 90% C.L. is determined for the BF ratio \mathcal{R} . For the normalization channel $\chi_{c1}(3872) \rightarrow \pi^+\pi^-J/\psi$, the total number of signal events ($N'_{\text{total}} = 86 \pm 10$) and the corresponding efficiencies are taken from Ref. [17]. The upper limit on \mathcal{R} at the 90% C.L. is defined as \mathcal{R}^{up} , corresponding to the value at 90% of the integral of the likelihood curve. The systematic uncertainty (cf. Table II) is also taken into account by applying a Gaussian smearing to the likelihood curve. The measured BF ratio is $\mathcal{R} = 0.04 \pm 0.06$, and the corresponding upper limit is set to $\mathcal{R} < 0.12$, as shown in Fig. 3.

In the BF ratio measurement, systematic uncertainties including the integrated luminosity, $e^+e^- \rightarrow \gamma\chi_{c1}(3872)$

TABLE II. Systematic uncertainties for the relative branching fraction \mathcal{R} measurement.

| Source | $\gamma\gamma$ | $\pi^+\pi^-\pi^0$ | Δ (%) |
|--|----------------|-------------------|--------------|
| Photon | | 2.0 | 2.0 |
| Tracking | 2.0 | 0.0 | 1.5 |
| $\mathcal{B}(\eta)$ | 0.5 | 1.2 | 0.7 |
| $\mathcal{B}(J/\psi \rightarrow l^+l^-)$ | | 0.6 | 0.6 |
| J/ψ mass window | | 1.6 | 1.6 |
| Decay model | 7.7 | 3.9 | 6.7 |
| η (π^0) reconstruction | | 1.0 | 1.0 |
| $\pi^+\pi^-J/\psi$ yield | | 12.3 | 12.3 |
| Total | | | 14.4 |

production cross section, radiative correction factor, tracking efficiency and photon detection, are cancelled. The remaining systematic uncertainties come from extra photon and track detection, BF, η (π^0) reconstruction, J/ψ mass window, MC decay model, signal extraction, and the uncertainty of $\chi_{c1}(3872)$ signal events in the $\pi^+\pi^-J/\psi$ mode.

In the $\chi_{c1}(3872) \rightarrow \pi^+\pi^-\eta$ decay, two more photons are detected. A 1.0% uncertainty is assigned to each photon [39], and the systematic uncertainty for photon detection is 2.0%. Similarly, there are only two charged tracks in the $\chi_{c1}(3872) \rightarrow \pi^+\pi^-\eta$ ($\rightarrow \gamma\gamma$) decay, while there are four in the $\chi_{c1}(3872) \rightarrow \pi^+\pi^-J/\psi$ ($\rightarrow \ell^+\ell^-$) decay. A 1.0% uncertainty [40] is assigned for each track, and in total 2.0% for the $\eta \rightarrow \gamma\gamma$ mode.

The uncertainties from $\mathcal{B}(\eta \rightarrow \gamma\gamma)$, $\mathcal{B}(\eta \rightarrow \pi^+\pi^-\pi^0)$, $\mathcal{B}(\pi^0 \rightarrow \gamma\gamma)$, and $\mathcal{B}(J/\psi \rightarrow l^+l^-)$ are not canceled out in the \mathcal{R} measurement. Systematic uncertainties are assigned according to PDG [7]. The systematic uncertainty due to η (π^0) reconstruction is also not cancelled out, and its contribution is 1.0% as mentioned before. The uncertainties

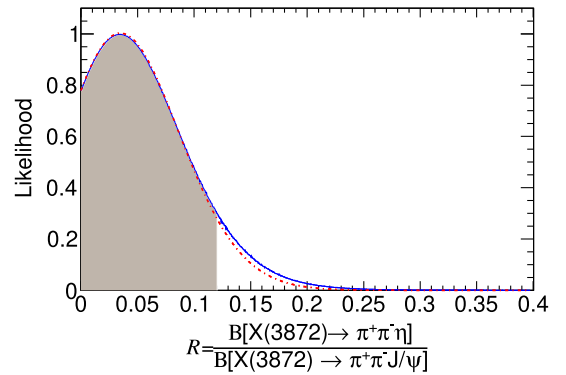


FIG. 3. The likelihood curve obtained by scanning various \mathcal{R} values in the fit. The red dot-dashed curve is from the nominal fit, the blue solid curve is the corresponding distribution smeared by a Gaussian function with resolution equal to the total systematic uncertainty, and the gray shaded area indicates 90% of the likelihood integral.

due to the $\chi_{c1}(3872) \rightarrow \pi^+\pi^-\eta$ decay model and $\chi_{c1}(3872)$ signal extraction are also discussed in the cross section measurement. In the $\chi_{c1}(3872) \rightarrow \pi^+\pi^-J/\psi$ decay, the systematic uncertainty due to the J/ψ mass window is 1.6% [17]. The uncertainties for the $\chi_{c1}(3872) \rightarrow \pi^+\pi^-J/\psi$ decay include the fit model, the background shape, and the statistical uncertainty of the signal yield, which have been studied in Ref. [17] and the combined contribution is 12.3%.

All the systematic uncertainties for the \mathcal{R} measurement are listed in Table II. The contributions from $\eta \rightarrow \gamma\gamma$ and $\pi^+\pi^-\pi^0$ modes are combined using the same method as the cross section measurement. Assuming all these sources are independent, the total systematic uncertainty is calculated by adding each individual source in quadrature.

In summary, we have searched for the decay $\chi_{c1}(3872) \rightarrow \pi^+\pi^-\eta$ associated with the radiative production $e^+e^- \rightarrow \gamma\chi_{c1}(3872)$ with 11.5 fb⁻¹ data at BESIII, at c.m. energies ranging from $\sqrt{s} = 4128.8$ MeV to 4337.9 MeV. No significant signal has been observed and the upper limits for the product of the production cross section and BF $\sigma[e^+e^- \rightarrow \gamma\chi_{c1}(3872)]\mathcal{B}[\chi_{c1}(3872) \rightarrow \pi^+\pi^-\eta]$ at 90% C.L. have been given. We have also measured the BF ratio $\mathcal{R} = \frac{\mathcal{B}[\chi_{c1}(3872) \rightarrow \pi^+\pi^-\eta]}{\mathcal{B}[\chi_{c1}(3872) \rightarrow \pi^+\pi^-J/\psi]}$, and set an upper limit $\mathcal{R} < 0.12$ at 90% C.L. Taking $\mathcal{B}[\chi_{c1}(3872) \rightarrow \pi^+\pi^-J/\psi] = (3.8 \pm 1.2)\%$ [7] as input, we obtain $\mathcal{B}[\chi_{c1}(3872) \rightarrow \pi^+\pi^-\eta] < 0.6\%$ at 90% C.L. A recent calculation assuming the $\chi_{c1}(3872)$ is a DD^* molecule state shows that the light hadron decay width of $\chi_{c1}(3872)$ is in the range of 10 keV to 10² keV [46] [corresponding to BF $\sim (1-10)\%$]. Since our measurement obviously finds the BF to be lower than 1%, this could have an impact on the explanation of the internal structure of the $\chi_{c1}(3872)$.

Acknowledgments. The BESIII Collaboration thanks the staff of BEPCII and the IHEP computing center for their strong support. This work is supported in part by National Key R&D Program of China under Contracts No. 2020YFA0406300 and No. 2020YFA0406400;

National Natural Science Foundation of China (NSFC) under Contracts No. 11975141, No. 11635010, No. 11735014, No. 11835012, No. 11935015, No. 11935016, No. 11935018, No. 11961141012, No. 12022510, No. 12025502, No. 12035009, No. 12035013, No. 12061131003, No. 12192260, No. 12192261, No. 12192262, No. 12192263, No. 12192264, No. 12192265, No. 12221005, No. 12225509 and No. 12235017; the Chinese Academy of Sciences (CAS) Large-Scale Scientific Facility Program; the CAS Center for Excellence in Particle Physics (CCEPP); Joint Large-Scale Scientific Facility Funds of the NSFC and CAS under Contract No. U1832207; CAS Key Research Program of Frontier Sciences under Contracts No. QYZDJ-SSW-SLH003 and No. QYZDJ-SSW-SLH040; 100 Talents Program of CAS; Project No. ZR2022JQ02 supported by Shandong Provincial Natural Science Foundation; Hubei University of Automotive Technology under Contract No. BK202318; The Institute of Nuclear and Particle Physics (INPAC) and Shanghai Key Laboratory for Particle Physics and Cosmology; ERC under Contract No. 758462; European Union's Horizon 2020 research and innovation programme under Marie Skłodowska-Curie Grant Agreement under Contract No. 894790; German Research Foundation DFG under Contracts No. 443159800 and No. 455635585, Collaborative Research Center CRC 1044, FOR5327, GRK 2149; Istituto Nazionale di Fisica Nucleare, Italy; Ministry of Development of Turkey under Contract No. DPT2006K-120470; National Research Foundation of Korea under Contract No. NRF-2022R1A2C1092335; National Science and Technology fund of Mongolia; National Science Research and Innovation Fund (NSRF) via the Program Management Unit for Human Resources & Institutional Development, Research and Innovation of Thailand under Contract No. B16F640076; Polish National Science Centre under Contract No. 2019/35/O/ST2/02907; The Swedish Research Council; U.S. Department of Energy under Contract No. DE-FG02-05ER41374.

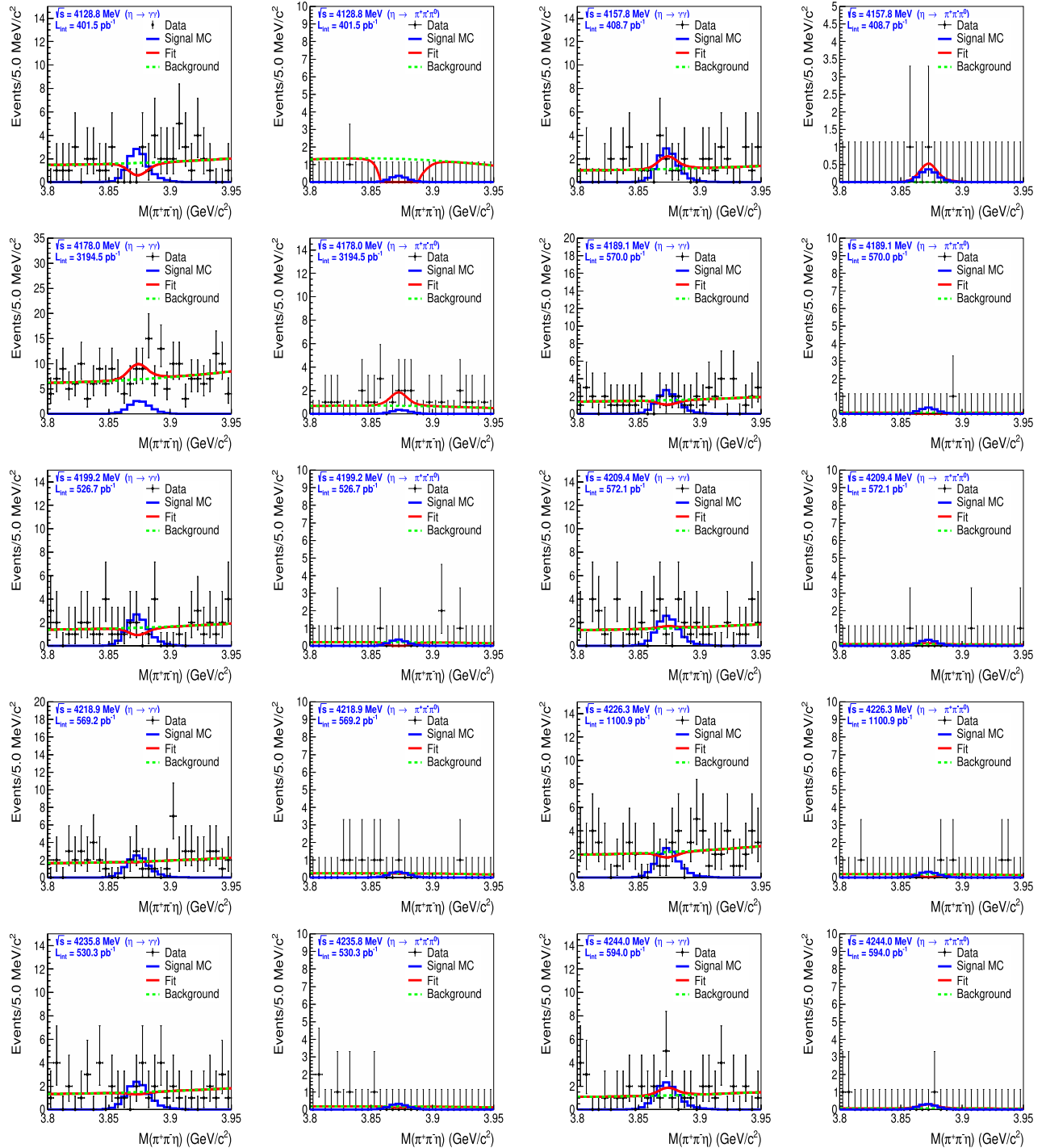
Appendix A: Fit to the $M(\pi^+\pi^-\eta)$ mass distribution at each c.m. energy.

FIG. 4. The fit results at c.m. energies ranging from $\sqrt{s} = 4128.8$ MeV to 4244.0 MeV. The signal MC shape convolved with a Gaussian function is used to fit the invariant mass spectrum of $\pi^+\pi^-\eta$ at each energy. Black dots with error bars are data, the red solid curve shows the fit result, the blue dashed curve is the signal contribution with arbitrary normalization and the green dashed curve is the background contribution.

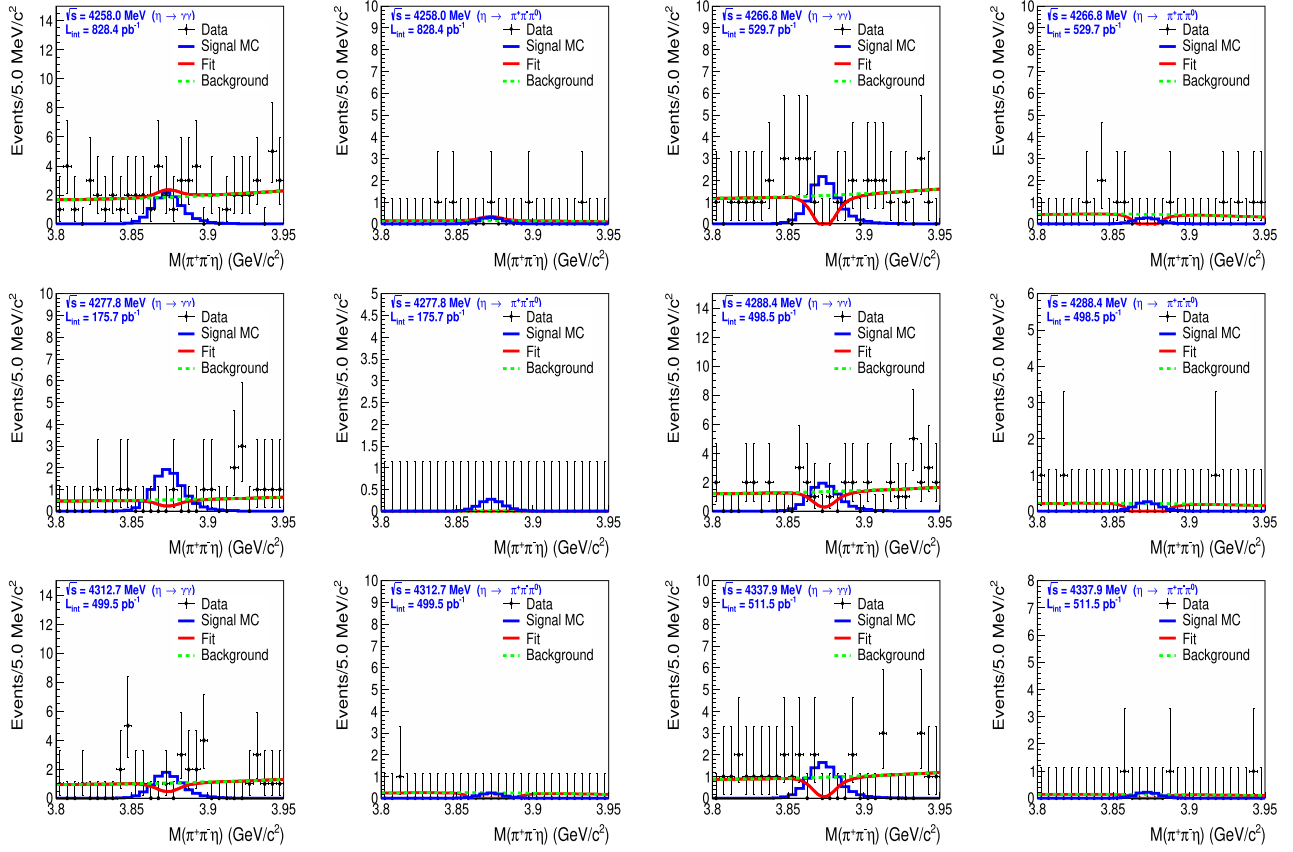


FIG. 5. The fit results at c.m. energies ranging from $\sqrt{s} = 4258.0$ MeV to 4337.9 MeV. The signal MC shape convolved with a Gaussian function is used to fit the invariant mass spectrum of $\pi^+\pi^-\eta$ at each energy. Black dots with error bars are data, the red solid curve shows the fit result, the blue dashed curve is the signal contribution with arbitrary normalization and the green dashed curve is the background contribution.

Appendix B: Systematic uncertainty at each c.m. energy.

TABLE III. Systematic uncertainties on the product of $(\sigma[e^+e^- \rightarrow \gamma\chi_{c1}(3872)]\mathcal{B}[\chi_{c1}(3872) \rightarrow \pi^+\pi^-\eta])^{\text{up}}$. Δ denotes the total systematic uncertainty. All entries are in percent.

| \sqrt{s} (MeV) | Photon | Tracking | Luminosity | Branching fraction | Kinematic fit | Decay model | ISR | $\eta(\pi^0)$ reconstruction | Δ |
|------------------|--------|----------|------------|--------------------|---------------|-------------|-----|------------------------------|----------|
| 4128.8 ± 0.4 | 3.0 | 2.5 | 0.7 | 0.7 | 2.0 | 5.6 | 0.3 | 1.0 | 7.2 |
| 4157.8 ± 0.3 | 3.0 | 2.5 | 0.7 | 0.7 | 1.8 | 5.6 | 0.6 | 1.0 | 7.2 |
| 4178.0 ± 0.8 | 3.0 | 2.5 | 0.7 | 0.7 | 2.1 | 6.0 | 0.9 | 1.0 | 7.6 |
| 4189.1 ± 0.3 | 3.0 | 2.5 | 0.7 | 0.7 | 1.9 | 5.2 | 1.1 | 1.0 | 7.0 |
| 4199.2 ± 0.3 | 3.0 | 2.5 | 0.7 | 0.7 | 2.0 | 6.2 | 1.3 | 1.0 | 7.8 |
| 4209.4 ± 0.3 | 3.0 | 2.5 | 0.7 | 0.7 | 1.9 | 5.0 | 1.2 | 1.0 | 6.9 |
| 4218.9 ± 0.3 | 3.0 | 2.5 | 0.7 | 0.7 | 1.8 | 6.4 | 1.0 | 1.0 | 7.9 |
| 4226.3 ± 0.7 | 3.0 | 2.5 | 0.7 | 0.7 | 2.0 | 5.8 | 1.0 | 1.0 | 7.5 |
| 4235.8 ± 0.3 | 3.0 | 2.5 | 0.7 | 0.7 | 2.0 | 6.2 | 1.1 | 1.0 | 7.8 |
| 4244.0 ± 0.3 | 3.0 | 2.5 | 0.7 | 0.7 | 1.8 | 6.0 | 0.9 | 1.0 | 7.6 |
| 4258.0 ± 0.7 | 3.0 | 2.5 | 0.7 | 0.7 | 1.7 | 5.2 | 0.9 | 1.0 | 6.9 |
| 4266.8 ± 0.3 | 3.0 | 2.5 | 0.7 | 0.7 | 2.1 | 4.8 | 0.9 | 1.0 | 6.7 |
| 4277.8 ± 0.5 | 3.0 | 2.5 | 0.7 | 0.7 | 2.0 | 4.1 | 0.8 | 1.0 | 6.2 |
| 4288.4 ± 0.3 | 3.0 | 2.5 | 0.7 | 0.7 | 2.0 | 6.2 | 0.7 | 1.0 | 7.7 |
| 4312.7 ± 0.4 | 3.0 | 2.5 | 0.7 | 0.7 | 1.7 | 5.8 | 0.6 | 1.0 | 7.4 |
| 4337.9 ± 0.4 | 3.0 | 2.5 | 0.7 | 0.7 | 1.7 | 5.6 | 0.4 | 1.0 | 7.2 |

- [1] S. K. Choi *et al.* (Belle Collaboration), *Phys. Rev. Lett.* **91**, 262001 (2003).
- [2] S. L. Olsen, T. Skwarnicki, and D. Zieminska, *Rev. Mod. Phys.* **90**, 015003 (2018); N. Brambilla, S. Eidelman, C. Hanhart, A. Nefediev, C.-P. Shen, C. E. Thomas, A. Vairo, and C.-Z. Yuan, *Phys. Rep.* **873**, 1 (2020).
- [3] L. Maiani, F. Piccinini, A. D. Polosa, and V. Riquer, *Phys. Rev. D* **71**, 014028 (2005); A. Esposito, A. L. Guerrieri, F. Piccinini, A. Pilloni, and A. D. Polosa, *Int. J. Mod. Phys. A* **30**, 1530002 (2015).
- [4] T. Barnes, S. Godfrey, and E. S. Swanson, *Phys. Rev. D* **72**, 054026 (2005).
- [5] E. S. Swanson, *Phys. Rep.* **429**, 243 (2006).
- [6] F. K. Guo, C. Hanhart, U. G. Meißner, Q. Wang, Q. Zhao, and B. S. Zou, *Rev. Mod. Phys.* **90**, 015004 (2018).
- [7] R. L. Workman *et al.* (Particle Data Group), *Prog. Theor. Exp. Phys.* **2022**, 083C01 (2022).
- [8] D. Acosta *et al.* (CDF II Collaboration), *Phys. Rev. Lett.* **93**, 072001 (2004); M. Aaboud *et al.* (ATLAS Collaboration), *J. High Energy Phys.* **01** (2017) 117; R. Aaij *et al.* (LHCb Collaboration), *J. High Energy Phys.* **01** (2022) 131; Y. J. Lee (CMS Collaboration), *Nucl. Phys.* **A1005**, 121781 (2021).
- [9] C. Bignamini, B. Grinstein, F. Piccinini, A. D. Polosa, and C. Sabelli, *Phys. Rev. Lett.* **103**, 162001 (2009).
- [10] M. Takizawa and S. Takeuchi, *Prog. Theor. Exp. Phys.* **2013**, 093D01 (2013).
- [11] R. Aaij *et al.* (LHCb Collaboration), *Phys. Rev. Lett.* **110**, 222001 (2013).
- [12] R. Aaij *et al.* (LHCb Collaboration), *Phys. Rev. D* **92**, 011102 (2015).
- [13] M. Ablikim *et al.* (BESIII Collaboration), *Phys. Rev. Lett.* **124**, 242001 (2020).
- [14] M. Ablikim *et al.* (BESIII Collaboration), *Phys. Rev. Lett.* **112**, 092001 (2014).
- [15] M. Ablikim *et al.* (BESIII Collaboration), *Phys. Rev. Lett.* **122**, 202001 (2019).
- [16] P. del Amo Sanchez *et al.* (BABAR Collaboration), *Phys. Rev. D* **82**, 011101 (2010).
- [17] M. Ablikim *et al.* (BESIII Collaboration), *Phys. Rev. Lett.* **122**, 232002 (2019).
- [18] V. Bhardwaj *et al.* (Belle Collaboration), *Phys. Rev. Lett.* **107**, 091803 (2011).
- [19] Y. Teramoto *et al.* (Belle Collaboration), *Phys. Rev. Lett.* **126**, 122001 (2021).
- [20] E. S. Swanson, *Phys. Lett. B* **598**, 197 (2004).
- [21] C. H. Li and C. Z. Yuan, *Phys. Rev. D* **100**, 094003 (2019).
- [22] M. Ablikim *et al.* (BESIII Collaboration), *Chin. Phys. C* **40**, 063001 (2016).
- [23] M. Ablikim *et al.* (BESIII Collaboration), *Chin. Phys. C* **45**, 103001 (2021).
- [24] M. Ablikim *et al.* (BESIII Collaboration), *Chin. Phys. C* **39**, 093001 (2015).
- [25] M. Ablikim *et al.* (BESIII Collaboration), *Chin. Phys. C* **41**, 063001 (2017).
- [26] M. Ablikim *et al.* (BESIII Collaboration), *Nucl. Instrum. Methods Phys. Res., Sect. A* **614**, 345 (2010).
- [27] C. H. Yu *et al.*, *Proceedings of IPAC2016, Busan, Korea* (2016), 10.18429/JACoW-IPAC2016-TUYA01.
- [28] M. Ablikim *et al.* (BESIII Collaboration), *Chin. Phys. C* **44**, 040001 (2020).
- [29] X. Li *et al.*, *Radiat. Detect. Technol. Methods* **1**, 13 (2017); Y. X. Guo *et al.*, *Radiat. Detect. Technol. Methods* **1**, 15 (2017); P. Cao *et al.*, *Nucl. Instrum. Methods Phys. Res., Sect. A* **953**, 163053 (2020).
- [30] S. Agostinelli *et al.* (GEANT4 Collaboration), *Nucl. Instrum. Methods Phys. Res., Sect. A* **506**, 250 (2003).
- [31] S. Jadach, B. F. L. Ward, and Z. Was, *Phys. Rev. D* **63**, 113009 (2001); *Comput. Phys. Commun.* **130**, 260 (2000).
- [32] D. J. Lange, *Nucl. Instrum. Methods Phys. Res., Sect. A* **462**, 152 (2001); R. G. Ping, *Chin. Phys. C* **32**, 599 (2008).
- [33] M. Ablikim *et al.* (BESIII Collaboration), *Phys. Rev. D* **92**, 012014 (2015); **107**, 092007 (2023).
- [34] E. Richter-Was, *Phys. Lett. B* **303**, 163 (1993).
- [35] J. C. Chen, G. S. Huang, X. R. Qi, D. H. Zhang, and Y. S. Zhu, *Phys. Rev. D* **62**, 034003 (2000); R. L. Yang, R. G. Ping, and H. Chen, *Chin. Phys. Lett.* **31**, 061301 (2014).
- [36] T. Sjöstrand, S. Ask, J. R. Christiansen, R. Corke, N. Desai, P. Ilten, S. Mrenna, S. Prestel, C. O. Rasmussen, and P. Z. Skands, *Comput. Phys. Commun.* **191**, 159 (2015).
- [37] L. Lista, *Lect. Notes Phys.* **909**, 1 (2016).
- [38] M. Ablikim *et al.* (BESIII Collaboration), *Chin. Phys. C* **46**, 113002 (2022).
- [39] M. Ablikim *et al.* (BESIII Collaboration), *Phys. Rev. D* **99**, 032001 (2019).
- [40] W. L. Yuan, X. C. Ai, X. B. Ji, S. J. Chen, Y. Zhang, L. H. Wu, L. L. Wang, and Y. Yuan, *Chin. Phys. C* **40**, 026201 (2016).
- [41] M. Ablikim *et al.* (BESIII Collaboration), *J. High Energy Phys.* **08** (2022) 196.
- [42] M. Ablikim *et al.* (BESIII Collaboration), *Phys. Rev. Lett.* **105**, 261801 (2010).
- [43] M. Ablikim *et al.* (BESIII Collaboration), *Phys. Rev. D* **87**, 012002 (2013).
- [44] W. Sun, T. Liu, M. Jing, L. Wang, B. Zhong, and W. Song, *Front. Phys. (Beijing)* **16**, 64501 (2021).
- [45] M. Ablikim *et al.* (BESIII Collaboration), *Phys. Rev. D* **95**, 032002 (2017).
- [46] Y. Wang, Q. Wu, G. Li, W. H. Qin, X. H. Liu, C. S. An, and J. J. Xie, *Phys. Rev. D* **106**, 074015 (2022).

M. Ablikim,¹ M. N. Achasov,^{5,b} P. Adlarson,⁷⁵ X. C. Ai,⁸¹ R. Aliberti,³⁶ A. Amoroso,^{74a,74c} M. R. An,⁴⁰ Q. An,^{71,58} Y. Bai,⁵⁷ O. Bakina,³⁷ I. Balossino,^{30a} Y. Ban,^{47,g} V. Batozskaya,^{1,45} K. Begzsuren,³³ N. Berger,³⁶ M. Berlowski,⁴⁵ M. Bertani,^{29a} D. Bettoni,^{30a} F. Bianchi,^{74a,74c} E. Bianco,^{74a,74c} A. Bortone,^{74a,74c} I. Boyko,³⁷ R. A. Briere,⁶ A. Brueggemann,⁶⁸ H. Cai,⁷⁶ X. Cai,^{1,58} A. Calcaterra,^{29a} G. F. Cao,^{1,63} N. Cao,^{1,63} S. A. Cetin,^{62a} J. F. Chang,^{1,58} T. T. Chang,⁷⁷ W. L. Chang,^{1,63}

G. R. Che,⁴⁴ G. Chelkov,^{37,a} C. Chen,⁴⁴ Chao Chen,⁵⁵ G. Chen,¹ H. S. Chen,^{1,63} M. L. Chen,^{1,58,63} S. J. Chen,⁴³ S. M. Chen,⁶¹ T. Chen,^{1,63} X. R. Chen,^{32,63} X. T. Chen,^{1,63} Y. B. Chen,^{1,58} Y. Q. Chen,³⁵ Z. J. Chen,^{26,h} W. S. Cheng,^{74c} S. K. Choi,¹¹ X. Chu,⁴⁴ G. Cibinetto,^{30a} S. C. Coen,⁴ F. Cossio,^{74c} J. J. Cui,⁵⁰ H. L. Dai,^{1,58} J. P. Dai,⁷⁹ A. Dbeysi,¹⁹ R. E. de Boer,⁴ D. Dedovich,³⁷ Z. Y. Deng,¹ A. Denig,³⁶ I. Denysenko,³⁷ M. Destefanis,^{74a,74c} F. De Mori,^{74a,74c} B. Ding,^{66,1} X. X. Ding,^{47,g} Y. Ding,⁴¹ Y. Ding,³⁵ J. Dong,^{1,58} L. Y. Dong,^{1,63} M. Y. Dong,^{1,58,63} X. Dong,⁷⁶ M. C. Du,¹ S. X. Du,⁸¹ Z. H. Duan,⁴³ P. Egorov,^{37,a} Y. L. Fan,⁷⁶ J. Fang,^{1,58} S. S. Fang,^{1,63} W. X. Fang,¹ Y. Fang,¹ R. Farinelli,^{30a} L. Fava,^{74b,74c} F. Feldbauer,⁴ G. Felici,^{29a} C. Q. Feng,^{71,58} J. H. Feng,⁵⁹ K. Fischer,⁶⁹ M. Fritsch,⁴ C. Fritsch,⁶⁸ C. D. Fu,¹ J. L. Fu,⁶³ Y. W. Fu,¹ H. Gao,⁶³ Y. N. Gao,^{47,g} Yang Gao,^{71,58} S. Garbolino,^{74c} I. Garzia,^{30a,30b} P. T. Ge,⁷⁶ Z. W. Ge,⁴³ C. Geng,⁵⁹ E. M. Gersabeck,⁶⁷ A. Gilman,⁶⁹ K. Goetzen,¹⁴ L. Gong,⁴¹ W. X. Gong,^{1,58} W. Gradl,³⁶ S. Gramigna,^{30a,30b} M. Greco,^{74a,74c} M. H. Gu,^{1,58} Y. T. Gu,¹⁶ C. Y. Guan,^{1,63} Z. L. Guan,²³ A. Q. Guo,^{32,63} L. B. Guo,⁴² M. J. Guo,⁵⁰ R. P. Guo,⁴⁹ Y. P. Guo,^{13,f} A. Guskov,^{37,a} T. T. Han,⁵⁰ W. Y. Han,⁴⁰ X. Q. Hao,²⁰ F. A. Harris,⁶⁵ K. K. He,⁵⁵ K. L. He,^{1,63} F. H. H. Heinsius,⁴ C. H. Heinz,³⁶ Y. K. Heng,^{1,58,63} C. Herold,⁶⁰ T. Holtmann,⁴ P. C. Hong,^{13,f} G. Y. Hou,^{1,63} X. T. Hou,^{1,63} Y. R. Hou,⁶³ Z. L. Hou,¹ H. M. Hu,^{1,63} J. F. Hu,^{56,i} T. Hu,^{1,58,63} Y. Hu,¹ G. S. Huang,^{71,58} K. X. Huang,⁵⁹ L. Q. Huang,^{32,63} X. T. Huang,⁵⁰ Y. P. Huang,¹ T. Hussain,⁷³ N. Hüsken,^{28,36} W. Imoehl,²⁸ J. Jackson,²⁸ S. Jaeger,⁴ S. Janchiv,³³ J. H. Jeong,¹¹ Q. Ji,¹ Q. P. Ji,²⁰ X. B. Ji,^{1,63} X. L. Ji,^{1,58} Y. Y. Ji,⁵⁰ X. Q. Jia,⁵⁰ Z. K. Jia,^{71,58} H. J. Jiang,⁷⁶ P. C. Jiang,^{47,g} S. S. Jiang,⁴⁰ T. J. Jiang,¹⁷ X. S. Jiang,^{1,58,63} Y. Jiang,⁶³ J. B. Jiao,⁵⁰ Z. Jiao,²⁴ S. Jin,⁴³ Y. Jin,⁶⁶ M. Q. Jing,^{1,63} T. Johansson,⁷⁵ X. K.,¹ S. Kabana,³⁴ N. Kalantar-Nayestanaki,⁶⁴ X. L. Kang,¹⁰ X. S. Kang,⁴¹ R. Kappert,⁶⁴ M. Kavatsyuk,⁶⁴ B. C. Ke,⁸¹ A. Khoukaz,⁶⁸ R. Kiuchi,¹ R. Kliemt,¹⁴ O. B. Kolcu,^{62a} B. Kopf,⁴ M. Kuessner,⁴ A. Kupsc,^{45,75} W. Kühn,³⁸ J. J. Lane,⁶⁷ P. Larin,¹⁹ A. Lavania,²⁷ L. Lavezzi,^{74a,74c} T. T. Lei,^{71,k} Z. H. Lei,^{71,58} H. Leithoff,³⁶ M. Lellmann,³⁶ T. Lenz,³⁶ C. Li,⁴⁸ C. Li,⁴⁴ C. H. Li,⁴⁰ Cheng Li,^{71,58} D. M. Li,⁸¹ F. Li,^{1,58} G. Li,¹ H. Li,^{71,58} H. B. Li,^{1,63} H. J. Li,²⁰ H. N. Li,^{56,i} Hui Li,⁴⁴ J. R. Li,⁶¹ J. S. Li,⁵⁹ J. W. Li,⁵⁰ K. L. Li,²⁰ Ke Li,¹ L. J. Li,^{1,63} L. K. Li,¹ Lei Li,³ M. H. Li,⁴⁴ P. R. Li,^{39,j,k} Q. X. Li,⁵⁰ S. X. Li,¹³ T. Li,⁵⁰ W. D. Li,^{1,63} W. G. Li,¹ X. H. Li,^{71,58} X. L. Li,⁵⁰ Xiaoyu Li,^{1,63} Y. G. Li,^{47,g} Z. J. Li,⁵⁹ Z. X. Li,¹⁶ C. Liang,⁴³ H. Liang,³⁵ H. Liang,^{71,58} H. Liang,^{1,63} Y. F. Liang,⁵⁴ Y. T. Liang,^{32,63} G. R. Liao,¹⁵ L. Z. Liao,^{50,m} Y. P. Liao,^{1,63} J. Libby,²⁷ A. Limphirat,⁶⁰ D. X. Lin,^{32,63} T. Lin,¹ B. J. Liu,¹ B. X. Liu,⁷⁶ C. Liu,³⁵ C. X. Liu,¹ F. H. Liu,⁵³ Fang Liu,¹ Feng Liu,⁷ G. M. Liu,^{56,i} H. Liu,^{39,j,k} H. B. Liu,¹⁶ H. M. Liu,^{1,63} Huanhuan Liu,¹ Huihui Liu,²² J. B. Liu,^{71,58} J. L. Liu,⁷² J. Y. Liu,^{1,63} K. Liu,¹ K. Y. Liu,⁴¹ Ke Liu,²³ L. Liu,^{71,58} L. C. Liu,⁴⁴ Lu Liu,⁴⁴ M. H. Liu,^{13,f} P. L. Liu,¹ Q. Liu,⁶³ S. B. Liu,^{71,58} T. Liu,^{13,f} W. K. Liu,⁴⁴ W. M. Liu,^{71,58} X. Liu,^{39,j,k} Y. Liu,⁸¹ Y. Liu,^{39,j,k} Y. B. Liu,⁴⁴ Z. A. Liu,^{1,58,63} Z. Q. Liu,⁵⁰ X. C. Lou,^{1,58,63} F. X. Lu,⁵⁹ H. J. Lu,²⁴ J. G. Lu,^{1,58} X. L. Lu,¹ Y. Lu,⁸ Y. P. Lu,^{1,58} Z. H. Lu,^{1,63} C. L. Luo,⁴² M. X. Luo,⁸⁰ T. Luo,^{13,f} X. L. Luo,^{1,58} X. R. Lyu,⁶³ Y. F. Lyu,⁴⁴ F. C. Ma,⁴¹ H. L. Ma,¹ J. L. Ma,^{1,63} L. L. Ma,⁵⁰ M. M. Ma,^{1,63} Q. M. Ma,¹ R. Q. Ma,^{1,63} R. T. Ma,⁶³ X. Y. Ma,^{1,58} Y. Ma,^{47,g} Y. M. Ma,³² F. E. Maas,¹⁹ M. Maggiora,^{74a,74c} S. Malde,⁶⁹ Q. A. Malik,⁷³ A. Mangoni,^{29b} Y. J. Mao,^{47,g} Z. P. Mao,¹ S. Marcello,^{74a,74c} Z. X. Meng,⁶⁶ J. G. Messchendorp,^{14,64} G. Mezzadri,^{30a} H. Miao,^{1,63} T. J. Min,⁴³ R. E. Mitchell,²⁸ X. H. Mo,^{1,58,63} N. Yu. Muchnoi,^{5,b} J. Muskalla,³⁶ Y. Nefedov,³⁷ F. Nerling,^{19,d} I. B. Nikolaev,^{5,b} Z. Ning,^{1,58} S. Nisar,^{12,1} Y. Niu,⁵⁰ S. L. Olsen,⁶³ Q. Ouyang,^{1,58,63} S. Pacetti,^{29b,29c} X. Pan,⁵⁵ Y. Pan,⁵⁷ A. Pathak,³⁵ P. Patteri,^{29a} Y. P. Pei,^{71,58} M. Pelizaeus,⁴ H. P. Peng,^{71,58} K. Peters,^{14,d} J. L. Ping,⁴² R. G. Ping,^{1,63} S. Plura,³⁶ S. Pogodin,³⁷ V. Prasad,³⁴ F. Z. Qi,¹ H. Qi,^{71,58} H. R. Qi,⁶¹ M. Qi,⁴³ T. Y. Qi,^{13,f} S. Qian,^{1,58} W. B. Qian,⁶³ C. F. Qiao,⁶³ J. J. Qin,⁷² L. Q. Qin,¹⁵ X. P. Qin,^{13,f} X. S. Qin,⁵⁰ Z. H. Qin,^{1,58} J. F. Qiu,¹ S. Q. Qu,⁶¹ C. F. Redmer,³⁶ K. J. Ren,⁴⁰ A. Rivetti,^{74c} V. Rodin,⁶⁴ M. Rolo,^{74c} G. Rong,^{1,63} Ch. Rosner,¹⁹ S. N. Ruan,⁴⁴ N. Salone,⁴⁵ A. Sarantsev,^{37,c} Y. Schelhaas,³⁶ K. Schoenning,⁷⁵ M. Scodreggio,^{30a,30b} K. Y. Shan,^{13,f} W. Shan,²⁵ X. Y. Shan,^{71,58} J. F. Shanguan,⁵⁵ L. G. Shao,^{1,63} M. Shao,^{71,58} C. P. Shen,^{13,f} H. F. Shen,^{1,63} W. H. Shen,⁶³ X. Y. Shen,^{1,63} B. A. Shi,⁶³ H. C. Shi,^{71,58} J. L. Shi,¹³ J. Y. Shi,¹ Q. Q. Shi,⁵⁵ R. S. Shi,^{1,63} X. Shi,^{1,58} J. J. Song,²⁰ T. Z. Song,⁵⁹ W. M. Song,^{35,1} Y. J. Song,¹³ Y. X. Song,^{47,g} S. Sosio,^{74a,74c} S. Spataro,^{74a,74c} F. Stielor,³⁶ Y. J. Su,⁶³ G. B. Sun,⁷⁶ G. X. Sun,¹ H. Sun,⁶³ H. K. Sun,¹ J. F. Sun,²⁰ K. Sun,⁶¹ L. Sun,⁷⁶ S. S. Sun,^{1,63} T. Sun,^{1,63} W. Y. Sun,³⁵ Y. Sun,¹⁰ Y. J. Sun,^{71,58} Y. Z. Sun,¹ Z. T. Sun,⁵⁰ Y. X. Tan,^{71,58} C. J. Tang,⁵⁴ G. Y. Tang,¹ J. Tang,⁵⁹ Y. A. Tang,⁷⁶ L. Y. Tao,⁷² Q. T. Tao,^{26,h} M. Tat,⁶⁹ J. X. Teng,^{71,58} V. Thoren,⁷⁵ W. H. Tian,⁵² W. H. Tian,⁵⁹ Y. Tian,^{32,63} Z. F. Tian,⁷⁶ I. Uman,^{62b} S. J. Wang,⁵⁰ B. Wang,¹ B. L. Wang,⁶³ Bo Wang,^{71,58} C. W. Wang,⁴³ D. Y. Wang,^{47,g} F. Wang,⁷² H. J. Wang,^{39,j,k} H. P. Wang,^{1,63} J. P. Wang,⁵⁰ K. Wang,^{1,58} L. L. Wang,¹ M. Wang,⁵⁰ Meng Wang,^{1,63} S. Wang,^{13,f} S. Wang,^{39,j,k} T. Wang,^{13,f} T. J. Wang,⁴⁴ W. Wang,⁵⁹ W. Wang,⁷² W. P. Wang,^{71,58} X. Wang,^{47,g} X. F. Wang,^{39,j,k} X. J. Wang,⁴⁰ X. L. Wang,^{13,f} Y. Wang,⁶¹ Y. D. Wang,⁴⁶ Y. F. Wang,^{1,58,63} Y. H. Wang,⁴⁸ Y. N. Wang,⁴⁶ Y. Q. Wang,¹ Yaqian Wang,^{18,1} Yi Wang,⁶¹ Z. Wang,^{1,58} Z. L. Wang,⁷² Z. Y. Wang,^{1,63} Ziyi Wang,⁶³ D. Wei,⁷⁰ D. H. Wei,¹⁵ F. Weidner,⁶⁸ S. P. Wen,¹ C. W. Wenzel,⁴ U. Wiedner,⁴ G. Wilkinson,⁶⁹ M. Wolke,⁷⁵ L. Wollenberg,⁴ C. Wu,⁴⁰ J. F. Wu,^{1,63} L. H. Wu,¹ L. J. Wu,^{1,63}

X. Wu,^{13,f} X. H. Wu,³⁵ Y. Wu,⁷¹ Y. J. Wu,³² Z. Wu,^{1,58} L. Xia,^{71,58} X. M. Xian,⁴⁰ T. Xiang,^{47,g} D. Xiao,^{39,j,k} G. Y. Xiao,⁴³
 S. Y. Xiao,¹ Y. L. Xiao,^{13,f} Z. J. Xiao,⁴² C. Xie,⁴³ X. H. Xie,^{47,g} Y. Xie,⁵⁰ Y. G. Xie,^{1,58} Y. H. Xie,⁷ Z. P. Xie,^{71,58}
 T. Y. Xing,^{1,63} C. F. Xu,^{1,63} C. J. Xu,⁵⁹ G. F. Xu,¹ H. Y. Xu,⁶⁶ Q. J. Xu,¹⁷ Q. N. Xu,³¹ W. Xu,^{1,63} W. L. Xu,⁶⁶ X. P. Xu,⁵⁵
 Y. C. Xu,⁷⁸ Z. P. Xu,⁴³ Z. S. Xu,⁶³ F. Yan,^{13,f} L. Yan,^{13,f} W. B. Yan,^{71,58} W. C. Yan,⁸¹ X. Q. Yan,¹ H. J. Yang,^{51,e} H. L. Yang,³⁵
 H. X. Yang,¹ Tao Yang,¹ Y. Yang,^{13,f} Y. F. Yang,⁴⁴ Y. X. Yang,^{1,63} Yifan Yang,^{1,63} Z. W. Yang,^{39,j,k} Z. P. Yao,⁵⁰ M. Ye,^{1,58}
 M. H. Ye,⁹ J. H. Yin,¹ Z. Y. You,⁵⁹ B. X. Yu,^{1,58,63} C. X. Yu,⁴⁴ G. Yu,^{1,63} J. S. Yu,^{26,h} T. Yu,⁷² X. D. Yu,^{47,g} C. Z. Yuan,^{1,63}
 L. Yuan,² S. C. Yuan,¹ X. Q. Yuan,¹ Y. Yuan,^{1,63} Z. Y. Yuan,⁵⁹ C. X. Yue,⁴⁰ A. A. Zafar,⁷³ F. R. Zeng,⁵⁰ X. Zeng,^{13,f}
 Y. Zeng,^{26,h} Y. J. Zeng,^{1,63} X. Y. Zhai,³⁵ Y. C. Zhai,⁵⁰ Y. H. Zhan,⁵⁹ A. Q. Zhang,^{1,63} B. L. Zhang,^{1,63} B. X. Zhang,¹
 D. H. Zhang,⁴⁴ G. Y. Zhang,²⁰ H. Zhang,⁷¹ H. H. Zhang,⁵⁹ H. H. Zhang,³⁵ H. Q. Zhang,^{1,58,63} H. Y. Zhang,^{1,58} J. J. Zhang,⁵²
 J. L. Zhang,²¹ J. Q. Zhang,⁴² J. W. Zhang,^{1,58,63} J. X. Zhang,^{39,j,k} J. Y. Zhang,¹ J. Z. Zhang,^{1,63} Jianyu Zhang,⁶³
 Jiawei Zhang,^{1,63} L. M. Zhang,⁶¹ L. Q. Zhang,⁵⁹ Lei Zhang,⁴³ P. Zhang,¹ Q. Y. Zhang,^{40,81} Shuihan Zhang,^{1,63}
 Shulei Zhang,^{26,h} X. D. Zhang,⁴⁶ X. M. Zhang,¹ X. Y. Zhang,⁵⁰ Xuyan Zhang,⁵⁵ Y. Zhang,⁷² Y. Zhang,⁶⁹ Y. T. Zhang,⁸¹
 Y. H. Zhang,^{1,58} Yan Zhang,^{71,58} Yao Zhang,¹ Z. H. Zhang,¹ Z. L. Zhang,³⁵ Z. Y. Zhang,⁷⁶ Z. Y. Zhang,⁴⁴ G. Zhao,¹ J. Zhao,⁴⁰
 J. Y. Zhao,^{1,63} J. Z. Zhao,^{1,58} Lei Zhao,^{71,58} Ling Zhao,¹ M. G. Zhao,⁴⁴ S. J. Zhao,⁸¹ Y. B. Zhao,^{1,58} Y. X. Zhao,^{32,63}
 Z. G. Zhao,^{71,58} A. Zhemchugov,^{37,a} B. Zheng,⁷² J. P. Zheng,^{1,58} W. J. Zheng,^{1,63} Y. H. Zheng,⁶³ B. Zhong,⁴² X. Zhong,⁵⁹
 H. Zhou,⁵⁰ L. P. Zhou,^{1,63} X. Zhou,⁷⁶ X. K. Zhou,⁷ X. R. Zhou,^{71,58} X. Y. Zhou,⁴⁰ Y. Z. Zhou,^{13,f} J. Zhu,⁴⁴ K. Zhu,¹
 K. J. Zhu,^{1,58,63} L. Zhu,³⁵ L. X. Zhu,⁶³ S. H. Zhu,⁷⁰ S. Q. Zhu,⁴³ T. J. Zhu,^{13,f} W. J. Zhu,^{13,f} Y. C. Zhu,^{71,58} Z. A. Zhu,^{1,63}
 J. H. Zou,¹ and J. Zu^{71,58}

(BESIII Collaboration)

¹*Institute of High Energy Physics, Beijing 100049, People's Republic of China*

²*Beihang University, Beijing 100191, People's Republic of China*

³*Beijing Institute of Petrochemical Technology, Beijing 102617, People's Republic of China*

⁴*Bochum Ruhr-University, D-44780 Bochum, Germany*

⁵*Budker Institute of Nuclear Physics SB RAS (BINP), Novosibirsk 630090, Russia*

⁶*Carnegie Mellon University, Pittsburgh, Pennsylvania 15213, USA*

⁷*Central China Normal University, Wuhan 430079, People's Republic of China*

⁸*Central South University, Changsha 410083, People's Republic of China*

⁹*China Center of Advanced Science and Technology, Beijing 100190, People's Republic of China*

¹⁰*China University of Geosciences, Wuhan 430074, People's Republic of China*

¹¹*Chung-Ang University, Seoul, 06974, Republic of Korea*

¹²*COMSATS University Islamabad, Lahore Campus, Defence Road, Off Raiwind Road, 54000 Lahore, Pakistan*

¹³*Fudan University, Shanghai 200433, People's Republic of China*

¹⁴*GSI Helmholtzcentre for Heavy Ion Research GmbH, D-64291 Darmstadt, Germany*

¹⁵*Guangxi Normal University, Guilin 541004, People's Republic of China*

¹⁶*Guangxi University, Nanning 530004, People's Republic of China*

¹⁷*Hangzhou Normal University, Hangzhou 310036, People's Republic of China*

¹⁸*Hebei University, Baoding 071002, People's Republic of China*

¹⁹*Helmholtz Institute Mainz, Staudinger Weg 18, D-55099 Mainz, Germany*

²⁰*Henan Normal University, Xinxiang 453007, People's Republic of China*

²¹*Henan University, Kaifeng 475004, People's Republic of China*

²²*Henan University of Science and Technology, Luoyang 471003, People's Republic of China*

²³*Henan University of Technology, Zhengzhou 450001, People's Republic of China*

²⁴*Huangshan College, Huangshan 245000, People's Republic of China*

²⁵*Hunan Normal University, Changsha 410081, People's Republic of China*

²⁶*Hunan University, Changsha 410082, People's Republic of China*

²⁷*Indian Institute of Technology Madras, Chennai 600036, India*

²⁸*Indiana University, Bloomington, Indiana 47405, USA*

^{29a}*INFN Laboratori Nazionali di Frascati, INFN Laboratori Nazionali di Frascati, I-00044, Frascati, Italy*

^{29b}*INFN Sezione di Perugia, I-06100, Perugia, Italy*

^{29c}*University of Perugia, I-06100, Perugia, Italy*

^{30a}*INFN Sezione di Ferrara, INFN Sezione di Ferrara, I-44122, Ferrara, Italy*

^{30b}*University of Ferrara, I-44122 Ferrara, Italy*

- ³¹Inner Mongolia University, Hohhot 010021, People's Republic of China
³²Institute of Modern Physics, Lanzhou 730000, People's Republic of China
³³Institute of Physics and Technology, Peace Avenue 54B, Ulaanbaatar 13330, Mongolia
³⁴Instituto de Alta Investigación, Universidad de Tarapacá, Casilla 7D, Arica 1000000, Chile
³⁵Jilin University, Changchun 130012, People's Republic of China
³⁶Johannes Gutenberg University of Mainz, Johann-Joachim-Becher-Weg 45, D-55099 Mainz, Germany
³⁷Joint Institute for Nuclear Research, 141980 Dubna, Moscow region, Russia
³⁸Justus-Liebig-Universitaet Giessen,
 II. Physikalisches Institut, Heinrich-Buff-Ring 16, D-35392 Giessen, Germany
³⁹Lanzhou University, Lanzhou 730000, People's Republic of China
⁴⁰Liaoning Normal University, Dalian 116029, People's Republic of China
⁴¹Liaoning University, Shenyang 110036, People's Republic of China
⁴²Nanjing Normal University, Nanjing 210023, People's Republic of China
⁴³Nanjing University, Nanjing 210093, People's Republic of China
⁴⁴Nankai University, Tianjin 300071, People's Republic of China
⁴⁵National Centre for Nuclear Research, Warsaw 02-093, Poland
⁴⁶North China Electric Power University, Beijing 102206, People's Republic of China
⁴⁷Peking University, Beijing 100871, People's Republic of China
⁴⁸Qufu Normal University, Qufu 273165, People's Republic of China
⁴⁹Shandong Normal University, Jinan 250014, People's Republic of China
⁵⁰Shandong University, Jinan 250100, People's Republic of China
⁵¹Shanghai Jiao Tong University, Shanghai 200240, People's Republic of China
⁵²Shanxi Normal University, Linfen 041004, People's Republic of China
⁵³Shanxi University, Taiyuan 030006, People's Republic of China
⁵⁴Sichuan University, Chengdu 610064, People's Republic of China
⁵⁵Soochow University, Suzhou 215006, People's Republic of China
⁵⁶South China Normal University, Guangzhou 510006, People's Republic of China
⁵⁷Southeast University, Nanjing 211100, People's Republic of China
⁵⁸State Key Laboratory of Particle Detection and Electronics,
 Beijing 100049, Hefei 230026, People's Republic of China
⁵⁹Sun Yat-Sen University, Guangzhou 510275, People's Republic of China
⁶⁰Suranaree University of Technology, University Avenue 111, Nakhon Ratchasima 30000, Thailand
⁶¹Tsinghua University, Beijing 100084, People's Republic of China
^{62a}Turkish Accelerator Center Particle Factory Group, Istinye University, 34010, Istanbul, Turkey
^{62b}Near East University, Nicosia, North Cyprus, 99138, Mersin 10, Turkey
⁶³University of Chinese Academy of Sciences, Beijing 100049, People's Republic of China
⁶⁴University of Groningen, NL-9747 AA Groningen, The Netherlands
⁶⁵University of Hawaii, Honolulu, Hawaii 96822, USA
⁶⁶University of Jinan, Jinan 250022, People's Republic of China
⁶⁷University of Manchester, Oxford Road, Manchester M13 9PL, United Kingdom
⁶⁸University of Muenster, Wilhelm-Klemm-Strasse 9, 48149 Muenster, Germany
⁶⁹University of Oxford, Keble Road, Oxford OX13RH, United Kingdom
⁷⁰University of Science and Technology Liaoning, Anshan 114051, People's Republic of China
⁷¹University of Science and Technology of China, Hefei 230026, People's Republic of China
⁷²University of South China, Hengyang 421001, People's Republic of China
⁷³University of the Punjab, Lahore-54590, Pakistan
^{74a}University of Turin and INFN, University of Turin, I-10125, Turin, Italy
^{74b}University of Eastern Piedmont, I-15121, Alessandria, Italy
^{74c}INFN, I-10125, Turin, Italy
⁷⁵Uppsala University, Box 516, SE-75120 Uppsala, Sweden
⁷⁶Wuhan University, Wuhan 430072, People's Republic of China
⁷⁷Xinyang Normal University, Xinyang 464000, People's Republic of China
⁷⁸Yantai University, Yantai 264005, People's Republic of China
⁷⁹Yunnan University, Kunming 650500, People's Republic of China
⁸⁰Zhejiang University, Hangzhou 310027, People's Republic of China
⁸¹Zhengzhou University, Zhengzhou 450001, People's Republic of China

^aAlso at the Moscow Institute of Physics and Technology, Moscow 141700, Russia.

^bAlso at the Novosibirsk State University, Novosibirsk 630090, Russia.

^cAlso at the NRC "Kurchatov Institute", PNPI, 188300, Gatchina, Russia.

^dAlso at Goethe University Frankfurt, 60323 Frankfurt am Main, Germany.

^eAlso at Key Laboratory for Particle Physics, Astrophysics and Cosmology, Ministry of Education; Shanghai Key Laboratory for Particle Physics and Cosmology; Institute of Nuclear and Particle Physics, Shanghai 200240, People's Republic of China.

^fAlso at Key Laboratory of Nuclear Physics and Ion-beam Application (MOE) and Institute of Modern Physics, Fudan University, Shanghai 200443, People's Republic of China.

^gAlso at State Key Laboratory of Nuclear Physics and Technology, Peking University, Beijing 100871, People's Republic of China.

^hAlso at School of Physics and Electronics, Hunan University, Changsha 410082, China.

ⁱAlso at Guangdong Provincial Key Laboratory of Nuclear Science, Institute of Quantum Matter, South China Normal University, Guangzhou 510006, China.

^jAlso at Frontiers Science Center for Rare Isotopes, Lanzhou University, Lanzhou 730000, People's Republic of China.

^kAlso at Lanzhou Center for Theoretical Physics, Lanzhou University, Lanzhou 730000, People's Republic of China.

^lAlso at the Department of Mathematical Sciences, IBA, Karachi 75270, Pakistan.

^mAlso at Hubei University of Automotive Technology, Shiyan 442002, People's Republic of China.